

Combination of Hidden Markov Random Field and Conjugate Gradient for Brain Image Segmentation

EL-Hachemi Guerrou¹, Samy Ait-Aoudia¹, Dominique Michelucci², and Ramdane Mahiou¹

¹ Ecole nationale Supérieure en Informatique, Laboratoire LMCS, Oued-Smar, Algiers, Algeria, {e.guerrou, s.ait_aoudia, r.mahiou}@esi.dz

² Université de Bourgogne, Laboratoire LE2I, Dijon, France, dominique.michelucci@u-bourgogne.fr

Abstract. Image segmentation is the process of partitioning the image into significant regions easier to analyze. Nowadays, segmentation has become a necessity in many practical medical imaging methods as locating tumors and diseases. Hidden Markov Random Field model is one of several techniques used in image segmentation. It provides an elegant way to model the segmentation process. This modeling leads to the minimization of an objective function. Conjugate Gradient algorithm (CG) is one of the best known optimization techniques. This paper proposes the use of the Conjugate Gradient algorithm (CG) for image segmentation, based on the Hidden Markov Random Field. Since derivatives are not available for this expression, finite differences are used in the CG algorithm to approximate the first derivative. The approach is evaluated using a number of publicly available images, where ground truth is known. The Dice Coefficient is used as an objective criterion to measure the quality of segmentation. The results show that the proposed CG approach compares favorably with other variants of Hidden Markov Random Field segmentation algorithms.

Keywords: Brain image segmentation, Hidden Markov Random Field, The Conjugate Gradient algorithm.

1 Introduction

Automatic segmentation of medical images becomes a crucial task due to the huge amount of data produced by imaging devices. Many popular tools as FSL [44] and Freesurfer [10] are dedicated to this aim.

There are several techniques to achieve the segmentation. We can broadly classify them into thresholding methods [21,28,45], clustering methods [31,41,6], edge detection methods [30,36,4], region-growing methods [22,34], watersheds methods [3,24], model-based methods [5,20,25,40] and Hidden Markov Random Field methods [44,19,29,13,17,1,14,15,16].

Threshold-based methods are the simplest ones that require only one pass through the pixels. They begin with the creation of an image histogram. After that, thresholds are used to separate the different image classes. For example, to segment an image into two classes, foreground and background, one threshold is necessary. The disadvantage of threshold-based techniques is the sensitivity to noise.

Region-based methods assemble neighboring pixels of the image in non-overlapping regions according to some homogeneity criterion. We distinguish two categories, region-growing methods and split-merge methods. They are effective when the neighboring pixels within one region have similar characteristics.

In model-based segmentation, a model is built for a specific anatomic structure by incorporating a prior information concerning shape, location and orientation. The presence of noise degrades the segmentation quality. This is why noise removal phase is generally an essential priority.

In classification methods, pixels are classified according to some properties or criteria: gray level, texture or color.

Hidden Markov Random Field (HMRF) [11] provides an elegant way to model the segmentation problem. It is based on the MAP (Maximum A Posteriori) criterion [42]. MAP estimation leads to the minimization of an objective function [39]. Therefore, optimization techniques are necessary to compute a solution. Conjugate Gradient Algorithm [26,33,37] is one of the most popular optimization methods.

This paper presents an automatic segmentation method based on the combination of Hidden Markov Field model and Conjugate Gradient algorithm. This method referred to as HMRF-CG, does not require preprocessing, feature extraction, training and learning. Brain MR image segmentation has attracted a particular attention in medical imaging. Thus, our tests rely on BrainWeb³ [7] and IBSR⁴ images where the ground truth is known. Segmentation quality is evaluated using Dice Coefficient (DC) [8] criterion. DC measures how much the segmentation result is close to the ground truth. This paper is organized as follows. We begin by introducing the concept of Hidden Markov Field in section 2. A short section 3 is devoted to the well known Conjugate Gradient algorithm. Section 4 is devoted to the experimental results and section 5 concludes the paper.

2 Hidden Markov Random Field (HMRF)

Let $S = \{s_1, s_2, \dots, s_M\}$ be the sites or positions set. Both image to segment and segmented image are formed of M sites. Each site $s \in S$ has a neighborhood set $V_s(S)$. A neighborhood system $V(S)$ has the following properties:

$$\begin{cases} \forall s \in S, s \notin V_s(S) \\ \forall \{s, t\} \in S, s \in V_t(S) \Leftrightarrow t \in V_s(S) \end{cases} \quad (1)$$

A r -order neighborhood system $V^r(S)$ is defined by the following formula:

$$V_s^r(S) = \{t \in S \mid \text{distance}(s, t)^2 \leq r^2 \wedge s \neq t\} \quad (2)$$

where $\text{distance}(s, t)$ is the Euclidean distance between pixels s and t . This distance depends only on the pixel position *i.e.*, it is not related to the pixel value. For volumetric data sets, as slices acquired by scanners, a 3D neighborhood system is used.

³ <http://www.bic.mni.mcgill.ca/brainweb/>

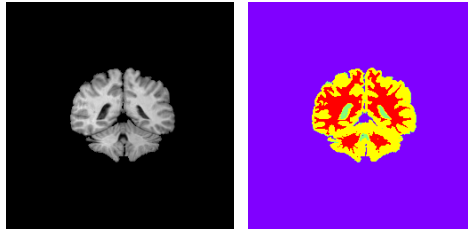
⁴ <https://www.nitrc.org/projects/ibsr>

A clique c is a subset of S where all sites are neighbors to each other. For a non single-site clique, we have:

$$\forall \{s, t\} \in c, s \neq t \Rightarrow (t \in V_s(S) \wedge s \in V_t(S)) \quad (3)$$

A p -order clique noted C_p contains p sites i.e. p is the cardinal of the clique.

Let $y = (y_1, y_2, \dots, y_M)$ be the pixels values of the image to segment and $x = (x_1, x_2, \dots, x_M)$ be the pixels classes of the segmented image. y_i and x_i are respectively pixel value and class of the site s_i . The image to segment y and the segmented image x are seen respectively as a realization of Markov Random families $Y = (Y_1, Y_2, \dots, Y_M)$ and $X = (X_1, X_2, \dots, X_M)$. The families of Random variables $\{Y_s\}_{s \in S}$ and $\{X_s\}_{s \in S}$ take their values respectively in the gray level space $E_y = \{0, \dots, 255\}$ and the discrete space $E_x = \{1, \dots, K\}$. K is the number of classes or homogeneous regions in the image. Configurations set of the image to segment y and the segmented image are respectively $\Omega_y = E_y^M$ and $\Omega_x = E_x^M$. Figure 1 shows an example of segmentation into four classes.



y : The image to segment x : The segmented image

Fig. 1. An example of segmentation with $K = 4$.

Segmentation of the image y consists in looking for a realization x of X . HMRF models this problem by maximizing the probability $P[X = x | Y = y]$.

$$x^* = \arg \max_{x \in \Omega_x} \{P[X = x | Y = y]\} \quad (4)$$

From the Bayes rule, we get:

$$P[X = x | Y = y] = \frac{P[Y = y | X = x] \times P[X = x]}{P[Y = y]} \quad (5)$$

Based on the conditional independence we have:

$$P[Y = y | X = x] = \prod_{s \in S} P[Y_s = y_s | X_s = x_s] \quad (6)$$

By the assumption that $P[Y_s = y_s | X_s = x_s]$ follows a normal distribution with mean μ_{x_s} and standard deviation σ_{x_s} , we will have:

$$P[Y_s = y_s | X_s = x_s] = \frac{1}{\sqrt{2\pi\sigma_{x_s}^2}} \exp\left(\frac{-(y_s - \mu_{x_s})^2}{2\sigma_{x_s}^2}\right) \quad (7)$$

According to equation 6 and 7 we get:

$$P[Y = y | X = x] = \prod_{s \in S} \frac{1}{\sqrt{2\pi\sigma_{x_s}^2}} \exp\left(\frac{-(y_s - \mu_{x_s})^2}{2\sigma_{x_s}^2}\right) \quad (8)$$

$$\Leftrightarrow P[Y = y | X = x] = (2\pi)^{\frac{-M}{2}} \exp\left(-\left(\sum_{s \in S} \left[\ln(\sigma_{x_s}) + \frac{(y_s - \mu_{x_s})^2}{2\sigma_{x_s}^2}\right]\right)\right) \quad (9)$$

where M is the image pixel number.

According to Hammersley-Clifford theorem [18] which establishes the equivalence between Markov field and Gibbs, we get:

$$P[X = x] = \frac{\exp\left(\frac{-U(x)}{T}\right)}{\sum_{\xi \in \Omega_x} \exp\left(\frac{-U(\xi)}{T}\right)} \quad (10)$$

where T is a control parameter called temperature.

The energy $U(x)$ is defined by Potts model [38] as follows:

$$U(x) = \beta \sum_{c_2 = \{s,t\}} (1 - 2\delta(x_s, x_t)) \quad (11)$$

where β is a constant and δ is the Kronecker's delta:

$$\delta(a, b) = \begin{cases} 1 & \text{if } a = b \\ 0 & \text{if } a \neq b \end{cases} \quad (12)$$

$P[Y = y]$ is a constant, so pose:

$$P[Y = y] = C \quad (13)$$

By replacing the equations (9), (10) and (13) in the equation (5), we will have:

$$\begin{cases} P[X = x | Y = y] = A \exp(-\Psi(x, y)) \\ \Psi(x, y) = \sum_{s \in S} \left[\ln(\sigma_{x_s}) + \frac{(y_s - \mu_{x_s})^2}{2\sigma_{x_s}^2}\right] + \frac{\beta}{T} \sum_{c_2 = \{s,t\}} (1 - 2\delta(x_s, x_t)) \\ A \text{ is a positive constant} \end{cases} \quad (14)$$

where T is a control parameter called temperature, δ is a Kronecker's delta and μ_{x_s} , σ_{x_s} are respectively the mean and standard deviation of the class x_s . When $\beta > 0$, the most likely segmentation corresponds to the constitution of large homogeneous regions. The size of these regions is controlled by the β value.

Maximizing the probability $P[X = x | Y = y]$ is equivalent to minimizing the function $\Psi(x, y)$.

$$x^* = \arg \min_{x \in \Omega_x} \{\Psi(x, y)\} \quad (15)$$

The computation of the exact segmentation x^* is impossible [11]. Therefore optimization techniques are necessary to compute an approximate solution \hat{x} .

Let $\mu = (\mu_1, \dots, \mu_j, \dots, \mu_K)$ be the means and $\sigma = (\sigma_1, \dots, \sigma_j, \dots, \sigma_K)$ be the standard deviations of K classes in the segmented image $x = (x_1, \dots, x_s, \dots, x_M)$ *i.e.*,

$$\begin{cases} \mu_j = \frac{1}{|S_j|} \sum_{s \in S_j} y_s \\ \sigma_j = \sqrt{\frac{1}{|S_j|} \sum_{s \in S_j} (y_s - \mu_j)^2} \\ S_j = \{s \mid x_s = j\} \end{cases} \quad (16)$$

Our way to minimize the function $\Psi(x, y)$ is to minimize instead the function $\Psi(\mu)$. We can always compute x through μ by classifying y_s into the nearest mean μ_j *i.e.*, $x_s = j$ if the nearest mean to y_s is μ_j . Thus instead of looking for x^* , we look for μ^* . The configuration set of μ is $\Omega_\mu = [0 \dots 255]^K$.

$$\begin{cases} \mu^* = \arg_{\mu \in \Omega_\mu} \min \{\Psi(\mu)\} \\ \Psi(\mu) = \sum_{j=1}^K \sum_{s \in S_j} [\ln(\sigma_j) + \frac{(y_s - \mu_j)^2}{2\sigma_j^2}] + \frac{\beta}{T} \sum_{c_2=\{s,t\}} (1 - 2\delta(x_s, x_t)) \end{cases} \quad (17)$$

where S_j , μ_j and σ_j are defined in the equation (16).

To apply unconstrained optimization techniques, we redefine the function $\Psi(\mu)$ for $\mu \in \mathbb{R}^K$ instead of $\mu \in \Omega_\mu$. Therefore, the new function $\Psi(\mu)$ becomes as follows:

$$\Psi(\mu) = \begin{cases} \sum_{j=1}^K \sum_{s \in S_j} [\ln(\sigma_j) + \frac{(y_s - \mu_j)^2}{2\sigma_j^2}] + \frac{\beta}{T} \sum_{c_2=\{s,t\}} (1 - 2\delta(x_s, x_t)) & \text{if } \mu \in \Omega_\mu \\ +\infty & \text{otherwise} \end{cases} \quad (18)$$

3 The Conjugate Gradient (CG) Algorithm

In practice, the application is implemented in the cross-platform Qt creator (C++) under Linux system. We have used the GNU Scientific Library implementation of Polak-Ribière Conjugate Gradient method [32,12] (`gsl_multimin_fdfminimizer_conjugate_pr`).

To use Conjugate Gradient Algorithm, we need the first derivative $\Psi'(\mu) = (d_1, \dots, d_i, \dots, d_n)$. Since no mathematical expression is available, it is approximated with finite differences [9] as follows:

– A forward difference approximation is

$$d_i = \frac{\Psi(\mu_1, \dots, \mu_i + \varepsilon, \dots, \mu_n) - \Psi(\mu_1, \dots, \mu_i, \dots, \mu_n)}{\varepsilon} \quad (19)$$

– A backward difference approximation is

$$d_i = \frac{\Psi(\mu_1, \dots, \mu_i, \dots, \mu_n) - \Psi(\mu_1, \dots, \mu_i - \varepsilon, \dots, \mu_n)}{\varepsilon} \quad (20)$$

– A centered difference approximation is

$$d_i = \frac{\Psi(\mu_1, \dots, \mu_i + \varepsilon, \dots, \mu_n) - \Psi(\mu_1, \dots, \mu_i - \varepsilon, \dots, \mu_n)}{2\varepsilon} \quad (21)$$

In our tests, we have used a centered difference approximation to compute the first derivative. The good approximation of the first derivative relies on the choice of the value of the parameter ε . Through the tests conducted, we have selected 0.01 as the best value.

4 Experimental Results

In this section, we begin by showing the effectiveness of HMRF-CG method. To this end, we will make a comparison with some methods (used in the field) that are: MRF-Classical [43], MRF-ACO-Gossiping [43] and MRF-ACO [35]. Secondly, we will show the robustness of HMRF-CG method against noise, by doing a comparison with LGMM method (Local Gaussian Mixture Model)[23]. The implementation of LGMM is built upon the segmentation method [2] of SPM 8 (Statistical Parametric Mapping⁵), which is a well known software for MRI analysis. As reported by [23], LGMM has better results than SPM 8.

To perform a fair and meaningful comparison, we have used a metric known as Dice Coefficient [8]. Morey et al. [27] used interchangeably Dice coefficient and Percentage volume overlap. This metric is usable only when the ground truth segmentation is known (see section 4.1). The image sets and related parameters are described in section 4.2. Finally, section 4.3 is devoted to the yielded results.

4.1 Dice Coefficient metric

Dice Coefficient (DC) measures how much the result is close to the ground truth. Let the resulting class be \hat{A} and its ground truth be A^* . Dice Coefficient is given by the following formula:

$$DC = \frac{2|\hat{A} \cap A^*|}{|\hat{A} \cup A^*|} = \frac{2TP}{2TP + FP + FN} \quad (22)$$

where TP stands for true positive, FP for false positive and FN for false negative. DC equals 1 in the best case *i.e.*, \hat{A} and A^* are identical and it equals 0 in the worst case *i.e.*, there is an empty intersection between \hat{A} and A^* .

⁵ <http://www.fil.ion.ucl.ac.uk/spm/software/spm8/>

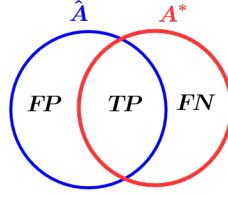


Fig. 2. TP, FP and FN.

4.2 The image sets and related parameters

To evaluate the quality of segmentation, we use four volumetric (3D) MR images, one obtained from IBSR (real image) and the others from BrainWeb (simulated images). Three components were considered: GM (Grey Matter), WM (White Matter) and CSF (Cerebro Spinal Fluid).

IBSR image dimension is $256 \times 256 \times 63$, with voxel= $1 \times 3 \times 1$ mm and T1-weighted modality. The three BrainWeb images dimensions are $181 \times 217 \times 181$, with voxels= $1 \times 1 \times 1$ mm and T1-weighted modality. We tested three levels of noise 0%, 3% and 5% with different intensity non-uniformity 0% and 20%.

In this paper we have retained a subset of slices, which are cited in [43]. The IBSR slices retained are: 1-24/18, 1-24/20, 1-24/24, 1-24/26, 1-24/30, 1-24/32 and 1-24/34. The BrainWeb slices retained are: 85, 88, 90, 95, 97, 100, 104, 106, 110, 121 and 130.

Table 1 defines some parameters necessary to execute HMRF-CG method.

Table 1. Related parameters to the images used in our tests.

Image	The constant β	The temperature T	The initial point μ^0
IBSR	1	10	(1, 5, 140, 190)
BrainWeb1		10	(1, 45, 110, 150)
BrainWeb2		4	
BrainWeb3		1	

4.3 Results

Table 2 shows the mean DC values using IBSR image. The parameters used by HMRF-CG are described in Table 1. The parameters used by the other methods are given in [43,35].

Table 3 shows the mean DC values using BrainWeb images. The parameters used by HMRF-CG are described in Table 1. The parameters used by the LGMM method are given in LGMM [23]. The column (N,I) gives noise and intensity non-uniformity.

Table 2. Mean DC values (the best results are given in bold type).

Methods	Dice Coefficient			
	GM	WM	CSF	Mean
Classical-MRF	0.771	0.828	0.253	0.617
MRF-ACO	0.778	0.827	0.263	0.623
MRF-ACO-Gossiping	0.778	0.827	0.262	0.623
HMRF-CG	0.859	0.855	0.381	0.698

Table 3. Mean DC values (the best results are in bold type).

Image	(N,I)	HMRF-CG				LGMM			
		Dice Coefficient				Dice Coefficient			
		GM	WM	CSF	Mean	GM	WM	CSF	Mean
BrainWeb1	(0%,0%)	0.970	0.990	0.961	0.974	0.697	0.667	0.751	0.705
BrainWeb2	(3%,20%)	0.940	0.965	0.940	0.949	0.905	0.940	0.897	0.914
BrainWeb3	(5%,20%)	0.918	0.952	0.924	0.931	0.912	0.951	0.893	0.918

Figure 3, Figure 4 and Figure 5 show respectively a sample of slices to segment obtained from IBSR image, a segmented slice using HMRF-CG method and a ground truths slice.

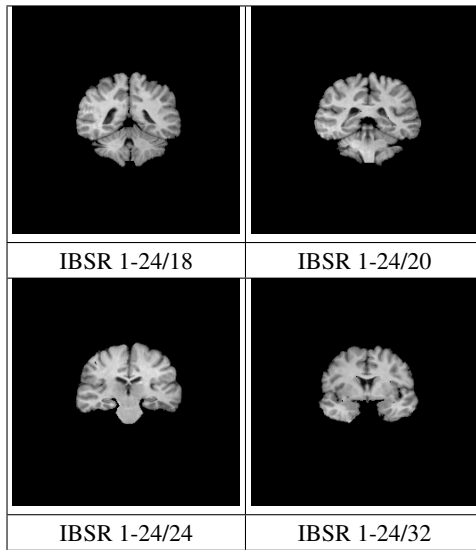


Fig. 3. A sample of slices to segment from IBSR image.

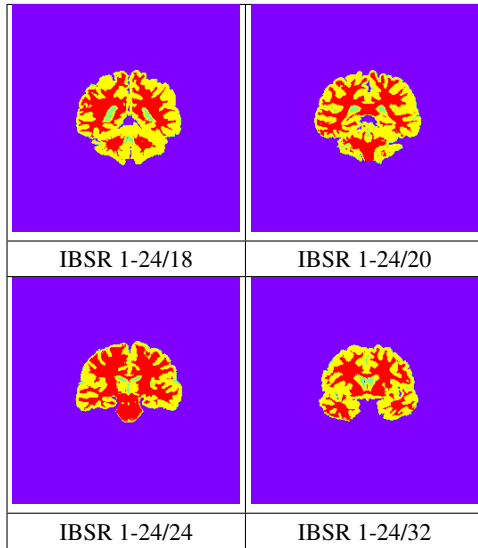


Fig. 4. A sample of segmented slices using HMRF-CG.

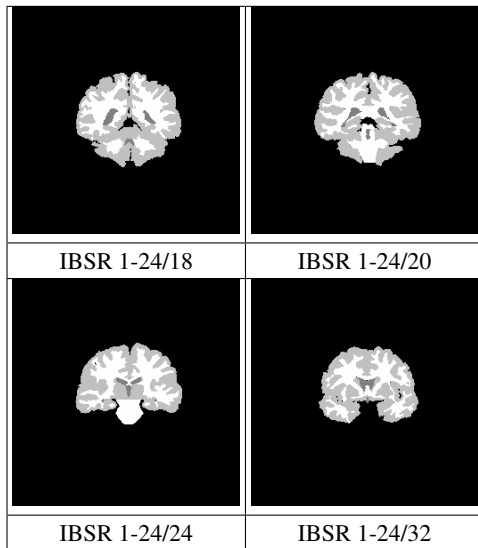


Fig. 5. A sample of ground truths images from IBSR image.

Figure 6 shows a sample of slices to segment from BrainWeb images and segmented slices using HMRF-CG. The column (N,I) gives noise and intensity non-uniformity.

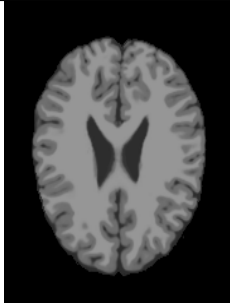
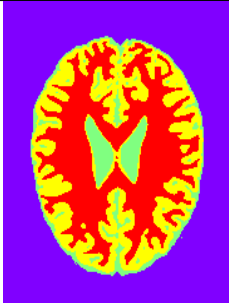
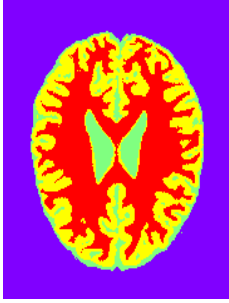
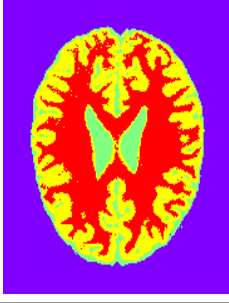
Image	(N,I)	Slice to segment	Segmented slice
BrainWeb1	(0%,0%)		
BrainWeb2	(3%,20%)		
BrainWeb3	(5%,20%)		

Fig. 6. The slices number #97 with different noise and intensity non-uniformity from BrainWeb images and their segmentation using HMRF-CG.

5 Discussion and Conclusion

In this paper, we have described a method which combines Hidden Markov Random Field (HMRF) and Conjugate Gradient (GC). The tests have been carried out on samples obtained from IBSR and BrainWeb images, the most commonly used images in the field. For a fair and meaningful comparison of methods, the segmentation quality is measured using the Dice Coefficient metric. The results depend on the choice of parameters. This very sensitive task has been conducted by performing numerous tests. From the results obtained, the HMRF-GC method outperforms the methods tested that are: LGMM, Classical MRF, MRF-ACO-Gossiping and MRF-ACO. Tests permit to

find good parameters for HMRF-CG to achieve good segmentation results. To further improve performances a preprocessing step can be added to reduce noise and inhomogeneity using appropriate filters.

Acknowledgment

We would like to thank BRAINWEB and IBSR communities for allowing us to use their images in the evaluation of brain segmentation.

References

1. Ait-Aoudia, S., Guerrou, E.H., Mahiou, R.: Medical image segmentation using particle swarm optimization. In: Information Visualisation (IV), 2014 18th International Conference on. pp. 287–291. IEEE (2014)
2. Ashburner, J., Friston, K.J.: Unified segmentation. *Neuroimage* 26(3), 839–851 (2005)
3. Benson, C., Lajish, V., Rajamani, K.: Brain tumor extraction from MRI brain images using marker based watershed algorithm pp. 318–323 (2015)
4. Canny, J.: A computational approach to edge detection. *Pattern Analysis and Machine Intelligence, IEEE Transactions on* (6), 679–698 (1986)
5. Chan, T.F., Vese, L., et al.: Active contours without edges. *Image processing, IEEE transactions on* 10(2), 266–277 (2001)
6. Chuang, K.S., Tzeng, H.L., Chen, S., Wu, J., Chen, T.J.: Fuzzy c-means clustering with spatial information for image segmentation. *computerized medical imaging and graphics* 30(1), 9–15 (2006)
7. Cocosco, C.A., Kollokian, V., Kwan, R.K.S., Pike, G.B., Evans, A.C.: Brainweb: Online interface to a 3d MRI simulated brain database (1997)
8. Dice, L.R.: Measures of the amount of ecologic association between species. *Ecology* 26(3), 297–302 (1945)
9. Eberly, D.: Derivative approximation by finite differences. Magic Software, Inc (2003)
10. Fischl, B.: Freesurfer. *Neuroimage* 62(2), 774–781 (2012)
11. Geman, S., Geman, D.: Stochastic relaxation, Gibbs distributions, and the bayesian restoration of images. *Pattern Analysis and Machine Intelligence, IEEE Transactions on* (6), 721–741 (1984)
12. Grippo, L., Lucidi, S.: A globally convergent version of the Polak-Ribière conjugate gradient method. *Mathematical Programming* 78(3), 375–391 (1997)
13. Guerrou, E., Ait-Aoudia, S., Michelucci, D., Mahiou, R.: Hidden markov random fields and direct search methods for medical image segmentation. In: Proceedings of the 5th International Conference on Pattern Recognition Applications and Methods. pp. 154–161 (2016)
14. Guerrou, E.H., Ait-Aoudia, S., Michelucci, D., Mahiou, R.: Hidden markov random field model and bfgs algorithm for brain image segmentation. In: Proceedings of the Mediterranean Conference on Pattern Recognition and Artificial Intelligence. pp. 7–11. MedPRAI-2016, ACM, New York, NY, USA (2016), <http://doi.acm.org/10.1145/3038884.3038886>
15. Guerrou, E.H., Mahiou, R., Ait-Aoudia, S.: Medical image segmentation on a cluster of pcs using markov random fields. *International Journal of New Computer Architectures and their Applications (IJNCAA)* 3(1), 35–44 (2013)

16. Guerrou, E.H., Mahiou, R., Ait-Aoudia, S.: Medical image segmentation using hidden markov random field a distributed approach. In: The Third International Conference on Digital Information Processing and Communications. pp. 423–430. The Society of Digital Information and Wireless Communication (2013)
17. Guerrou, E.H., Mahiou, R., Ait-Aoudia, S.: Hidden markov random fields and swarm particles: a winning combination in image segmentation. IERI Procedia 10, 19–24 (2014)
18. Hammersley, J.M., Clifford, P.: Markov fields on finite graphs and lattices (1971)
19. Held, K., Kops, E.R., Krause, B.J., Wells III, W.M., Kikinis, R., Muller-Gartner, H.W.: Markov random field segmentation of brain MR images. Medical Imaging, IEEE Transactions on 16(6), 878–886 (1997)
20. Ho, S., Bullitt, L., Gerig, G.: Level-set evolution with region competition: automatic 3-d segmentation of brain tumors 1, 532–535 (2002)
21. Kumar, S., et al.: Skull stripping and automatic segmentation of brain MRI using seed growth and threshold techniques pp. 422–426 (2007)
22. Lin, G.C., Wang, W.J., Kang, C.C., Wang, C.M.: Multispectral MR images segmentation based on fuzzy knowledge and modified seeded region growing. Magnetic resonance imaging 30(2), 230–246 (2012)
23. Liu, J., Zhang, H.: Image segmentation using a local gmm in a variational framework. Journal of mathematical imaging and vision 46(2), 161–176 (2013)
24. Masoumi, H., Behrad, A., Pourmina, M.A., Roosta, A.: Automatic liver segmentation in MRI images using an iterative watershed algorithm and artificial neural network. Biomedical Signal Processing and Control 7(5), 429–437 (2012)
25. McInerney, T., Terzopoulos, D.: Deformable models in medical image analysis: a survey. Medical image analysis 1(2), 91–108 (1996)
26. Møller, M.F.: A scaled conjugate gradient algorithm for fast supervised learning. Neural networks 6(4), 525–533 (1993)
27. Morey, R.A., Petty, C.M., Xu, Y., Hayes, J.P., Wagner, H.R., Lewis, D.V., LaBar, K.S., Styner, M., McCarthy, G.: A comparison of automated segmentation and manual tracing for quantifying hippocampal and amygdala volumes. Neuroimage 45(3), 855–866 (2009)
28. Natarajan, P., Krishnan, N., Kenkre, N.S., Nancy, S., Singh, B.P.: Tumor detection using threshold operation in MRI brain images pp. 1–4 (2012)
29. Panjwani, D.K., Healey, G.: Markov random field models for unsupervised segmentation of textured color images. Pattern Analysis and Machine Intelligence, IEEE Transactions on 17(10), 939–954 (1995)
30. Perona, P., Malik, J.: Scale-space and edge detection using anisotropic diffusion. Pattern Analysis and Machine Intelligence, IEEE Transactions on 12(7), 629–639 (1990)
31. Pham, D.L., Xu, C., Prince, J.L.: Current methods in medical image segmentation 1. Annual review of biomedical engineering 2(1), 315–337 (2000)
32. Polak, E., Ribière, G.: Note sur la convergence de méthodes de directions conjuguées. Revue française d'informatique et de recherche opérationnelle, série rouge 3(1), 35–43 (1969)
33. Powell, M.J.D.: Restart procedures for the conjugate gradient method. Mathematical programming 12(1), 241–254 (1977)
34. Roura, E., Oliver, A., Cabezas, M., Vilanova, J.C., Rovira, À., Ramió-Torrentà, L., Lladó, X.: Marga: multispectral adaptive region growing algorithm for brain extraction on axial MRI. Computer methods and programs in biomedicine 113(2), 655–673 (2014)
35. Salima, O., Mohamed, B.: MRF-based image segmentation using ant colony system 2, 012–24 (2003)
36. Senthilkumaran, N., Rajesh, R.: Edge detection techniques for image segmentation—a survey of soft computing approaches. International journal of recent trends in engineering 1(2) (2009)

37. Shewchuk, J.R.: An introduction to the conjugate gradient method without the agonizing pain. Lecture available on internet (1994)
38. Swendsen, R.H., Wang, J.S.: Nonuniversal critical dynamics in Monte Carlo simulations. *Physical review letters* 58(2), 86 (1987)
39. Szeliski, R., Zabih, R., Scharstein, D., Veksler, O., Kolmogorov, V., Agarwala, A., Tappen, M., Rother, C.: A comparative study of energy minimization methods for Markov random fields with smoothness-based priors. *Pattern Analysis and Machine Intelligence, IEEE Transactions on* 30(6), 1068–1080 (2008)
40. Wang, L., Shi, F., Li, G., Gao, Y., Lin, W., Gilmore, J.H., Shen, D.: Segmentation of neonatal brain MR images using patch-driven level sets. *NeuroImage* 84, 141–158 (2014)
41. Wu, Z., Leahy, R.: An optimal graph theoretic approach to data clustering: Theory and its application to image segmentation. *Pattern Analysis and Machine Intelligence, IEEE Transactions on* 15(11), 1101–1113 (1993)
42. Wyatt, P.P., Noble, J.A.: MAP MRF joint segmentation and registration of medical images. *Medical Image Analysis* 7(4), 539–552 (2003)
43. Yousefi, S., Azmi, R., Zahedi, M.: Brain tissue segmentation in MR images based on a hybrid of MRF and social algorithms. *Medical image analysis* 16(4), 840–848 (2012)
44. Zhang, Y., Brady, M., Smith, S.: Segmentation of brain mr images through a hidden markov random field model and the expectation-maximization algorithm. *IEEE transactions on medical imaging* 20(1), 45–57 (2001)
45. Zhao, M., Lin, H.Y., Yang, C.H., Hsu, C.Y., Pan, J.S., Lin, M.J.: Automatic threshold level set model applied on MRI image segmentation of brain tissue. *Appl. Math* 9(4), 1971–1980 (2015)